Current Chemistry Letters 14 (2025) 867–884

Contents lists available at GrowingScience

Current Chemistry Letters

homepage: www.GrowingScience.com

1,2,4-triazole-chalcone and derivatives as antiproliferative agents: Quantum chemical studies, molecular docking, ADME-Tox and MD simulation

Hanane Zaki[a], Mohamed Ouabane[b], Soumaya Aissaoui[a], Marwa Alaqarbeh[c] and Mohammed Bouachrine[b*]

[a]*Biotechnology, Bioresources, and Bioinformatics Laboratory, Higher School of Technology, University of Sultan My Slimane, PB 170, Khenifra 54000 Morocco*
[b]*Molecular Chemistry and Natural Substances Laboratory, Faculty of Science, Moulay Ismail University of Meknes, B.P. 11201, Meknes, Morocco*
[c]*Department of Chemistry, Faculty of Science, Applied Science Private University, Amman, 11931, Jordan*

C H R O N I C L E

Article history:
Received March 10, 2025
Received in revised form
June 2, 2025
Accepted July 7, 2025
Available online
July 7, 2025

Keywords:
1,2,4-triazole-chalcone
Antiproliferative activity
Molecular Docking
MD Simulation

A B S T R A C T

The investigation of 1,2,4-triazole-chalcone has sparked immense interest due to their promising biological activities. These compounds, labeled 10C-10S, were synthesized and characterized by Jinjing et al., specifically focusing on their potential applications in biological settings, particularly their antiproliferative properties. Strategic exploration by computational chemistry techniques such as DFT calculations, molecular docking, and molecular dynamics with empirical findings proved pivotal in unraveling the multifaceted properties of these organic molecules. Additionally, molecular docking studies were conducted to elucidate the antiproliferative effects and analyze the potential binding modes of the compounds with specific amino acid residues in proteins. Rigorous comparisons between theoretical and experimental results yielded comprehensive insights into the properties of these compounds. We chose two molecules, C (the most active) and E (the least active), which have affinities of -7.689 and -7.526 kcal/mol, respectively, to test how stable they are with the EGFR receptor (PDB entry code: 6Z4B). Molecular dynamics simulations over 100 ns revealed more stable energies, with ΔG_Bind = -25.135 Kcal/mol and ΔG_Bind_vdW = -30.644 Kcal/mol.

© 2025 by the authors; licensee Growing Science, Canada.

1. Introduction

Chalcone is a chemical compound easily modified with chemical groups and substituents[1]. This property enables it to interact with various molecular targets and exhibit diverse biological activities[2]. Several research studies have highlighted the potential of chalcone derivatives as anticancer compounds that induce tumor cell apoptosis[3]. Triazoles have significant pharmaceutical applications as anticancer drugs[4], aromatase inhibitors[5], protein kinase inhibitors[6], and carbonic anhydrase inhibitors[7]. The most common cancer drugs that contain triazole include 1,2,4-triazole, such as anastrozole and furosol[15]. Their distinct properties arise from their aromatic ring structure, heteroatoms, pi-conjugated system, and ability to act as hydrogen bond donors and acceptors[8]. They also engage in various interactions, including Van der Waals forces, pi stacking, hydrophobic interactions, and strong binding to metals[9]. A newly synthesized [1,2,4] triazolo[3,4-b] [1,3,4] thiadiazol and chalcone compound by Ericsson et al., were examined through *in-vitro* experiments on four human tumor cell lines: HCT116 (human colon cancer cells), HT29 (human colon cancer cells), human non-small cell lung cancer cells, HeLa (human cervical cancer cells), and MCF-7 (human breast cancer cells)[10]. The results demonstrate promising inhibitory effects against human colon cancer cells (HCT116)[11].

The current study aims to investigate the structures of [1,2,4] triazolo[3,4-b] [1,3,4] thiadiazol and chalcone compounds synthesized by Ericsson et al. (**Fig. 1**), as well as the interactions between the chalcone-based molecules and their respective receptors[12]. Employing DFT quantum chemical methods with functional B3LYP 6–31G (d, p) levels of theory is crucial for

* Corresponding author
E-mail address m.bouachrine@umi.ac.ma (M. Bouachrine)

© 2025 by the authors; licensee Growing Science, Canada
doi: 10.5267/j.ccl.2025.7.002

exploring the physiochemical properties of organic molecules[13]. Subsequent *in-silico* studies utilizing molecular docking and molecular dynamic simulations were conducted to elucidate experimental findings' biological effects and propose potential interactions and bindings between the target compounds (ligands) and the active amino acids derived from the respective proteins[14]. The results from molecular docking, dynamic simulations, and quantum studies were compared with experimental data to validate and support the findings.

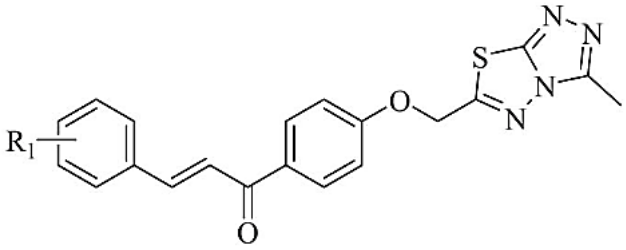

Fig. 1. Studied compounds (A-E)
(A): R_1= 2-fluloro; (B): R_1= 5-bromo-2-chloro; (C): R_1= 4-dimethylamino; (D): 2-formyl-3-(4-formylthiophen-2-yl); (E): R_1= 2-formyl-3-(4-methylthiophen-2-yl).

2. Materials and Methods

2.1. Data set

The chemical data with their reported antiproliferative activities were taken from the literature[15]. Antiproliferative activities of the studied chalcone compounds A to E against the human colon cancer cell SW620. Compound C showed good antiproliferative activity against the SW620 cell line, and its IC_{50} value was 21.55 μM. According to the results, the antiproliferative activity of this series of compounds was evaluated in SW620 (human colon cancer cells) using the MTT method with cisplatin as the positive control drug. The obtained biological activity values are listed with their corresponding structures in **Table 1.**

Table 1. Anti-proliferative activities against SW620 cell line (mm)[10]

Studied Compounds	10c (A)	10g (B)	10o (C)	10q (D)	10s (E)
IC_{50} (mM)	28.26	23.28	21.55	35.22	33.35

2.2. DFT calculations

This study used the hybrid functional Becke three parameters B3 with the nonlocal correlation of Lee-Yang-Parr LYP called B3LYP method (B3LYP)[16]. The 6-31G (d, p) basis set was used for all calculations[17]. The density (DFT) functional calculations are performed using the Gaussian 09 package[18]. It is noted that the use of this method and this basis set appears to be an adequate approach for the study of physicochemical compounds and most organic compounds[19]. This method introduces electron correlation effects at a lower cost in the computation's time. The geometry structures of neutral molecules (A, B, C, D, and E) were optimized under no constraint. Also, HOMO and LUMO levels were determined of the molecules studied; the Egap energy, which was evaluated as the difference between the HOMO and LUMO energy levels, and other electronic parameters were also determined.

2.3. Molecular Docking Protocol

Molecular docking was performed to investigate the interactions between the studied compounds (A, B, C, D, and E) and the epidermal growth factor receptor (EGFR), aiming to validate and elucidate the experimental results[20]. The anti-EGFR compounds are designed to bind to EGFR, obstructing growth factor binding, receptor activation, and subsequent signal transduction events that lead to cell proliferation. Given the critical role of EGFR in anticancer therapy, predicting the binding modes of these compounds is essential. The crystal structure of EGFR (PDB entry code: 6Z4B) was downloaded from the Protein Data Bank, and the original ligands, Osimertinib and EAI045, were removed to allow docking of our DFT-optimized compounds (A, B, C, D, and E)[21]. The docking protocol involved several steps. First, the EGFR crystal structure was prepared by removing co-crystallized ligands and water molecules using Discovery Studio software[22]. This prepared structure was saved in PDB format for use in docking studies. Molecular docking simulations were then conducted with MOE.2014, starting with adjustments to the backbone structure[23]. Atomic charges and parameters were optimized using the MMFF94x force field, and the protein and ligand structures were saved in MDB format[24]. The protein PDB files were configured by adding non-polar hydrogen atoms, selecting the receptor, and creating α-site spheres using the active site search tool[25]. During the docking analysis, after 500 trials, the most stable anchor sites were identified in the protein's inner grooves. London's ΔG scoring function was used to calculate scoring energies, with two triangular matching methods refining the results[26]. The analysis considered interaction planes, electrostatics, and key interaction parameters. Factors such as specific amino acids in the ligand and receptor structures, interaction types, internal and scoring energies, and binding

lengths of 3.5 Å or less were evaluated to ensure accurate results for assessing the inhibition potential of the five compounds[27].

2.4. ADME-Tox Prediction

The ADME-Tox properties of the investigated molecules were predicted using the SWISS ADME Predictor tool, which assesses the pharmacokinetics, drug compatibility, and suitability of small molecules[28]. The optimized structures of the molecules were used to predict various physicochemical properties such as lipophilicity, water solubility, pharmacokinetics, and drug compatibility[29]. This information is essential for predicting the behavior of molecules and guiding the selection of the best leads[30]. Indeed, a critical step in drug discovery is the optimization of candidate chemical structures according to their ADMET parameters, considering pharmacokinetic properties[31]. Computer modeling provides valuable data on intestinal absorption, blood-brain barrier penetration, metabolic biotransformation, overall clearance, and potential toxicity of compounds. For this analysis, we used online pkCSM algorithms to predict the ADMET properties of the most suitable compounds[32].

2.3. Molecular Dynamics Simulations

The molecular system was prepared for molecular dynamics in this section of the dynamic simulation by following several essential steps using Schrödinger Maestro 2018-4. Initially, the bond order was assigned while importing and processing, a zero-order bond was created for the metal, and a disulfide bond was generated. Additionally, water molecules larger than 5.00 angstroms and their corresponding ion states were generated at pH 7 using Epik[33]. In the refinement phase, optimization was used to simplify the orientation of the water and reduce the number of hydrogens in the modified species[34]. The PRPKA model was used at pH 7 to account for the effects of the ionic environment. Further minimization was then performed, removing water molecules with less than three hydrogen bonds with non-water molecules to reduce solvation artifacts[35]. In addition, heavy atoms were converged to an RMSD of 0.3 Angstroms to ensure optimal system geometry[36]. Additional hydrogens were selectively added to optimize hydrogen interactions, and the OPLS3e force field was used to describe atomic interactions within the system accurately[37]. These methodological refinement steps are critical to ensuring the reliability of the dynamic simulation results[38]. The system configuration was established with an orthorhombic box shape, setting the dimensions a, b, and c to 10 angstroms to minimize the volume. Ions were added to achieve a concentration of 0.15 M NaCl[39]. The model system is prepared for simulation with a total duration of 100 ns, recording trajectory every 4.8 ps, and recording energy every 1.2 ps, resulting in around 500 frames. The ensemble class is set to Normal Pressure and Temperature (NPT), with a temperature of 300 K and a pressure of 1.01325 bar. We also conducted a system relaxation process to ensure a stable initial configuration before commencing the simulation. These methodological steps are crucial in establishing optimal conditions for a reliable dynamic simulation of the molecular system under study[40].

Prime MM-GBSA (Molecular Mechanics Generalized Born Surface Area) calculates a series of energy properties to assess ligand-receptor interactions, providing details on various aspects of binding and strain[41]. The five elemental energies calculated are the optimized energies for the free rPrime MM-GBSA (Molecular Mechanics Generalized Born Surface Area) calculates a series of energy properties to evaluate interactions between a ligand and receptor, providing details on various aspects of binding and strain[37]. The five basic energies calculated are the optimized energies for the free receptor, the free ligand, and their combined complex, as well as the receptor and ligand energies extracted from the minimized/optimized complex. Strain energies are then derived from these data, including Rec Strain (the difference in energy between the receptor in the optimized complex and the free receptor) and Lig Strain (the difference between the ligand in the optimized complex and the free ligand)[42]. The binding energy reflects the total interaction between the receptor and ligand and is calculated as the difference between the energy of the complex and the sum of the energies of the free receptor and the free ligand (MMGBSA ΔG Bind). This involves subtracting the energies of the receptor and ligand, which are extracted from the minimized/optimized complex, from the energy of the combined complex. From these data, strain energies are derived. These include Rec Strain (the difference in energy between the receptor in the optimized complex and the free receptor) and Lig Strain (the difference between the ligand in the optimized complex and the free ligand). The binding energy reflects the total binding interaction and is calculated as the energy of the complex minus the energies of the free receptor and ligand (MMGBSA dG Bind)[43]. The MMGBSA dG Bind (NS), or 'stress-free' binding energy, excludes conformational changes in the receptor and ligand and provides a measure of the binding affinity without the effects of stress. It also reports energy contributions from various components, including coulomb, covalent, van der Waals, solv-gb, hydrogen bonds, packing, and self-contact. The energy properties are presented in the project table with names formatted as calculation-type components, where calculation-type indicates the energy type and component's contribution. The most important properties are 'MMGBSA dG Bind' and 'Prime Energy' (the energy of the complex).

3. Results

3.1. DFT results

To characterize the studied molecules theoretically, the chemical structure and electronic properties of the target molecules were optimized to understand the correlation between structure and properties. The optimized structure geometries obtained by B3LYP/6-31G (d, p) of all studied molecules (A, B, C, D, and E) are shown in **Fig. 2**.

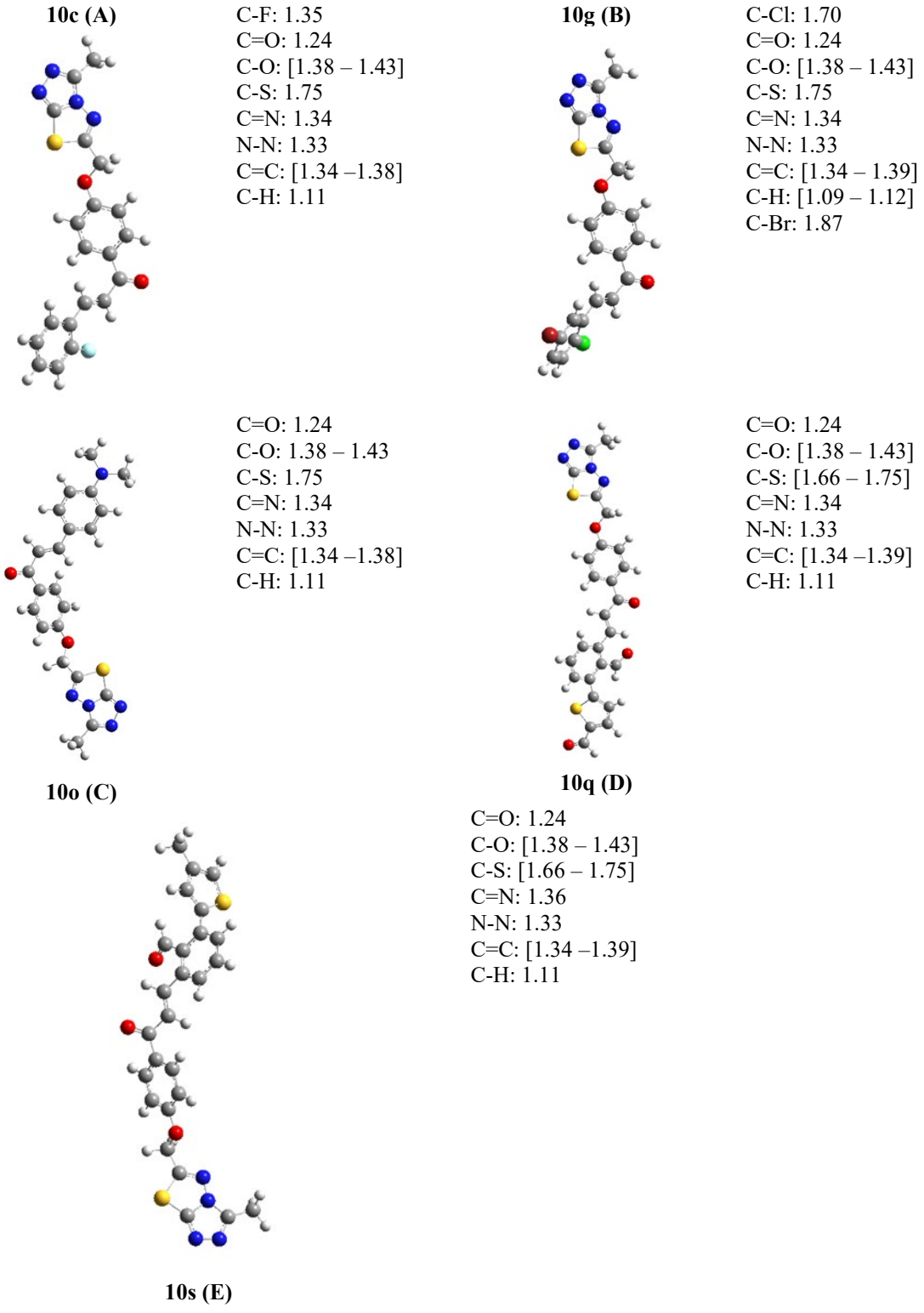

Fig. 2. Optimized geometric structures of studied compounds, and bond lengths (Å)

Understanding the distribution in the highest occupied molecular orbital (HOMO) and lowest unoccupied molecular orbital (LUMO) shows how stable and reactive the compounds being studied are chemically. The properties of these occupied and unoccupied orbitals make it possible to predict the most reactive sites and explain the reaction mechanisms. It also explains the properties of the studied molecules and their interactions with biological receptors[44]. The calculation of HOMO and LUMO energies can be done from the electrochemical potential of oxidation and reduction. While theoretically accessible, these properties are also accessible by DFT quantum calculation. The (HOMO) measures the electron-donor character, or the ability to donate an electron, while the (LUMO) measures the electron-acceptor character, or the ability to obtain an electron.

In **Fig. 3**, we have presented the places of the orbital lobes HOMO and LUMO of our compounds. These orbitals have similar electronic distributions, regardless of the compound under study. The electron distribution of HOMOs of all compounds presents the anti-bonding character between the two adjacent fragments. Meanwhile, the electron distribution of LUMOs presents the bonding character between the two adjacent fragments.

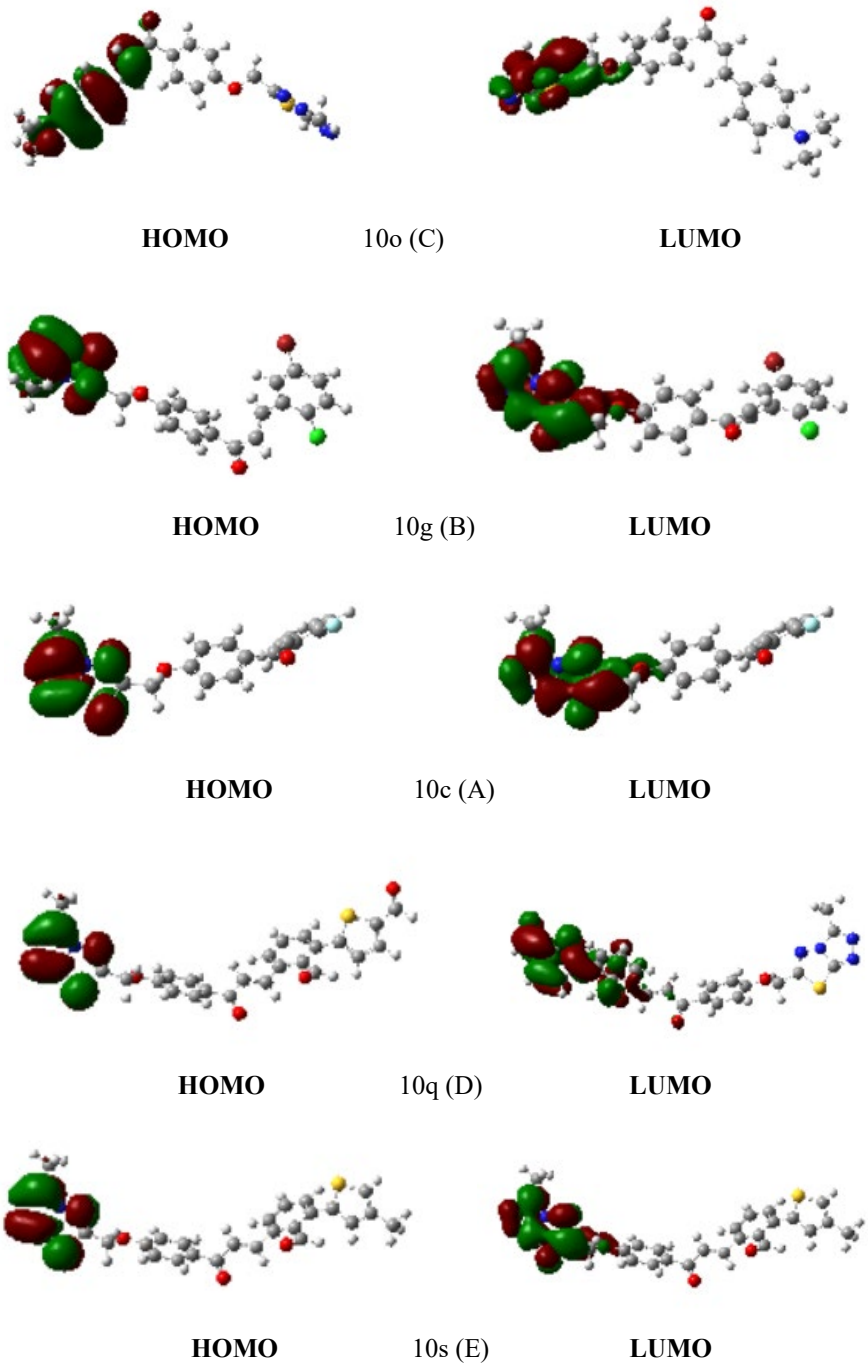

Fig. 3. Schematic representations of HOMO and LUMO molecular orbitals of studied molecules obtained with DFT at the B3LYP/6-31G (d, p) level.

On the other hand, the energy gap is an interesting parameter that can explain the different electronic properties, reactivity, and stability of any compound[45]. A small band gap facilitates the transport of electrons from the HOMO level to the LUMO level when the molecule absorbs light of a particular wavelength. At the same time, a significant gap contributes to good electronic stability[46]. Therefore, the energies of HOMO, LUMO, and the gap energy were determined from the DFT-optimized structure of the studied compounds (see Table 2). We have also calculated other chemical descriptors such as the ionization potential (I), the electron affinity (A), the chemical hardness (η), and the softness (r) according to Koopman's theorem[47].

- The ionization potential (**I**): **$I = - E_{HOMO}$**;
- The electron affinity (**A**): **$A = - E_{LUMO}$**;
- The chemical hardness (η): $\eta = 1/2 (- A + I) = (E_{LUMO} - E_{HOMO})$;
- The softness (ρ): $\rho = 1/\eta$.

Table 2. Quantum chemical parameters for the studied compounds obtained with the DFT at the B3LYP/6-31G (d, p) level

Compounds	E_{HOMO} (eV)	E_{LUMO} (eV)	Egap (eV)	Hardness (η)	Softness ($\square$)	Dipole moment, μ (Debye)
A	-2.39	-6.51	4.41	2.21	0.45	3.40
B	-2.33	-6.68	4.35	2.18	0.46	3.00
C	-1.69	-5.30	3.61	1.80	0.56	7.02
D	-2.68	-6.68	4.00	2.00	0.50	4.79
E	-2.38	-6.23	3.85	1.93	0.52	6.05

It is known that the energy of (E_{HOMO}) measures the tendency towards donating electrons, while the E_{LUMO} indicates the ability to accept electrons. Therefore, the obtained values of (E_{HOMO}, E_{LUMO}) are (-2.39, -6.51); (-2.33, -6.69); (-1.69, -5.30); (-2.68, -6.68) and (-2.38, -6.23) for A, B, C, D, and E respectively. We have noted that:

- ✓ The high value of the HOMO energy and the low value of the LUMO energy are probably responsible for the high activity of the compound C;
- ✓ Concerning the energy gap value ΔE, larger energy difference values reflect low reactivity and high stability. C's low band gap value indicates that this molecule has high reactivity. This compound C has the particularity of containing a dimethylamino group known for its electron-donor properties in its structure. Especially since these dimethylamino groups seem to be of great structural importance in inhibiting the antiproliferative activity of cancer cells;
- ✓ It is confirmed by the low obtained value of hardness and the high obtained value of softness, and it means that the molecule C could have better performance as a ligand.
- ✓ Dipole moment, μ(Debye), is another important parameter that results from the non-uniform distribution of charges on the various atoms in the molecule. The high value of μ(Debye) probably increases the interaction between the molecule and the protein and increases the activity of the studied ligands. In our study, we have calculated the dipole moment of the studied molecules. The results show that the most active molecule, C, has a dipole moment of 7.02 D.

On the other hand, it was noticed during the experimental study that the antiproliferative activity of compound B (IC_{50} = 23.28 µM) containing two halogen atoms is better than that of compound A (IC_{50} = 28.26 µM), which contains a halogen atom. This is well confirmed by DFT studies, where compound B has a gap energy of 4.30 eV lower than that of compound A (4.40 eV). The same observations for the properties of hardness and softness. This finding strongly agrees with the experimental results.

Molecular electrostatic potential:

The electronic charge distribution and relative sites of chemical reactivity of the molecule are represented by the molecular electrostatic potential (MEP) surface. This surface can predict electrophilic and nucleophilic active sites, determine a molecule's relative polarity, predict its reactive site, and visualize its charge distribution in three dimensions 2. As shown in **Fig. 4**, the MEP was calculated using B3LYP/6-31G (d, p) for the studied compounds.

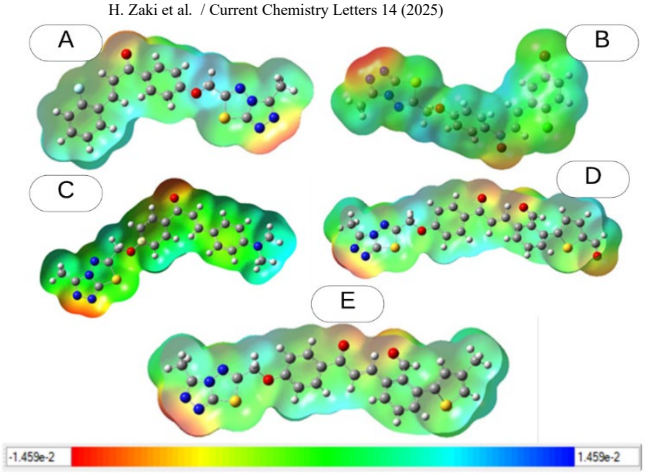

Fig. 4. ESP results of the studied molecules

The relative sizes of a molecule's chemical reactivity and polarity can be ascertained by examining the three-dimensional surface representation of the electronic charge distribution, or MEP. The maps that are produced when MEP is computed in this work utilizing the B3LYP/6-31G (d, p) approach are shown in Figure 4. With the highest electron density areas displayed in red and the lowest electron density areas displayed in blue, the maps display the MEP surfaces for each molecule. Predicting the molecules' reactive sites can be aided by the MEP maps, which offer information about the molecules' electrophilic and nucleophilic active sites. When it comes to attachment and luring prospective electrophiles, structures with negative regions correlate well with the chemicals under study.

3.2. Molecular docking results

The molecular docking analysis was carried out for the studied compounds (compounds A, B, C, D, and E) with the epidermal-growth-factor-receptor (EGFR) (PDB entry code: 6Z4B). EGFR functions as a tyrosine kinase receptor in the cell membrane and is activated in response to growth factors such as transforming growth factor (TGF)-a or EGF. These growth factors bind to the extracellular region of the receptor. The signaling process is then completed. The identification of EGFR as a potential target for therapeutic intervention arises from significant observations made in laboratory experiments and clinical settings. Initially, preclinical investigations demonstrated that EGFR activation plays a central role in promoting various tumorigenic processes. It includes stimulation of proliferation, angiogenesis, metastasis, and protection against apoptosis. Furthermore, monoclonal antibodies (MAbs) designed to target EGFR effectively inhibited EGFR-induced cell proliferation. As a result, various strategies have been developed to counteract EGFR, focusing on distinct elements within the EGFR signaling network[48].

Table 3. Molecular docking results (positions, affinity, and energy scores of ligands and complexes)

Ligands	X	Y	Z	Affinity Kcal/mol	Rmsd-refine	E-Conf	E-Place	E-Score1	E-Refine	E-Score2
C	**44.73**	**-4.69**	**-1.81**	**-7.69**	**2.54**	**103.83**	**-31.52**	**-6.97**	**-12.74**	**-7.69**
C	49.05	-7.71	-4.22	-7.34	2.56	90.69	-33.52	-6.50	-25.15	-7.34
C	44.62	-6.38	-2.36	-7.33	1.75	96.81	-43.67	-5.28	-13.71	-7.33
C	44.97	-7.76	-3.33	-7.25	1.80	89.30	-36.74	-7.85	-23.36	-7.25
C	45.09	-7.49	-3.58	-7.23	2.78	89.24	-39.79	-8.84	-19.23	-7.23
Ref	**45.98**	**-14.59**	**-5.25**	**-7.38**	**2.21**	**11.42**	**-16.79**	**-5.82**	**-25.42**	**-7.38**
Ref	49.80	-11.05	-3.92	-7.26	2.10	8.58	-39.98	-9.13	-24.97	-7.26
Ref	51.73	-11.84	-6.61	-7.20	2.09	13.48	-14.58	-8.42	-24.43	-7.20
Ref	57.79	-9.24	-7.62	-7.01	2.36	19.10	-17.25	-5.98	-21.58	-7.01
Ref	51.33	-11.91	-6.17	-6.70	1.50	9.74	-61.98	-9.37	-22.97	-7.00
E	**51.69**	**-9.64**	**-5.79**	**-7.53**	**2.64**	**124.88**	**-49.75**	**-5.12**	**-29.08**	**-7.53**
E	45.92	-9.27	-3.75	-7.45	3.36	123.26	-24.65	-5.10	-22.23	-7.45
E	45.03	-10.22	-3.43	-7.43	2.61	122.52	-38.42	-9.11	-24.93	-7.43
E	44.08	-10.47	-2.77	-7.23	4.62	128.65	-25.77	-3.69	-15.59	-7.23
E	45.65	-13.42	-4.65	-6.96	1.77	125.50	-44.54	-5.46	-23.04	-6.96

The results in docking **Table 3**, obtained using MOE.2014 software, show the binding affinities and different energy scores for three ligands: C, Ref, and E. Ligand C has coordinates (X: 44.73, Y: -4.69, Z: -1.81) and an affinity score of -7.69, with an Rmsd-refine of 2.54 and a high E-Conf value of 103.83. The E-Place and E-Score1 values are -31.52 and -6.97 respectively, indicating favorable binding placement and a positive initial score, while the E-Refine and E-Score2 values are -12.74 and -7.69. The reference ligand (Ref) has coordinates (X: 45.98, Y: -14.59, Z: -5.25), an affinity score of -7.38, with an Rmsd-refine of 2.21 and a low E-Conf value of 11.42. The E-Place and E-Score1 values are -16.79 and -5.82, with E-Refine and E-Score2 values of -25.42 and -7.38. Ligand E, with coordinates (X: 51.69, Y: -9.64, Z: -5.79), has an affinity score of -7.53, an Rmsd-refine of 2.64, and the highest E-Conf value of 124.88. The E-Place, E-Score1, E-Refine,

and E-Score2 values are -49.75, -5.12, -29.08, and -7.53 respectively. Overall, these results suggest that ligand E has the highest conformational energy and the best binding placement score, while ligand C shows the best affinity and a favorable initial score, indicating potentially strong binding interactions for both ligands.

3.3. Results of ligand-protein interactions:

3.3.1. Results of C molecule interactions

Molecular docking results indicate that the C molecule can bind to the target protein with high affinity. The interactions observed between the C molecule and the target protein are hydrogen bonds, electrostatic interactions, and hydrophobic interactions (**Fig. 5**).

Hydrogen bonds:

A hydrogen bond is present between the H46 of the C molecule and an oxygen atom and the target protein's amino acid isoleucine 759 (ILE759) with a 2.886 Å distance. This interaction is essential for stabilizing the ligand-protein complex. Electrostatic interactions: pi-cation-type electrostatic interaction was observed between the target protein's C molecule and the amino acid lysine 745 (LYS745), with 4.956 Å. This interaction is formed by the attraction between the positive charge of the nitrogen atom of the pyridinium ring of the C molecule and the negative charge of the oxygen atom of the carboxyl group of the LYS745 amino acid.

Hydrophobic interactions:

Several hydrophobic interactions are present between the C molecule and the amino acids of the target protein. An alkyl-type hydrophobic interaction is observed between the C44 atom of molecule C and the Cβ atom of the amino acid alanine 763 (ALA763) of the target protein, with a 3.476 Å distance. The carbon atom (C37) of the C molecule and the S atom of the target protein's amino acid cysteine 797 (CYS797) have a 4.296-Å alkyl-type hydrophobic interaction. Other hydrophobic interactions of the alkyl and pi-alkyl types were observed between the C molecule and the amino acids ILE759, LEU788, LEU861, ILE759, LEU861, LEU862, MET766, LEU777, LEU788, LEU858, VAL726, ALA743, LYS745, LEU844 and CYS797 of the target protein, with distances of between 4.082 Å and 5.485 Å, respectively.

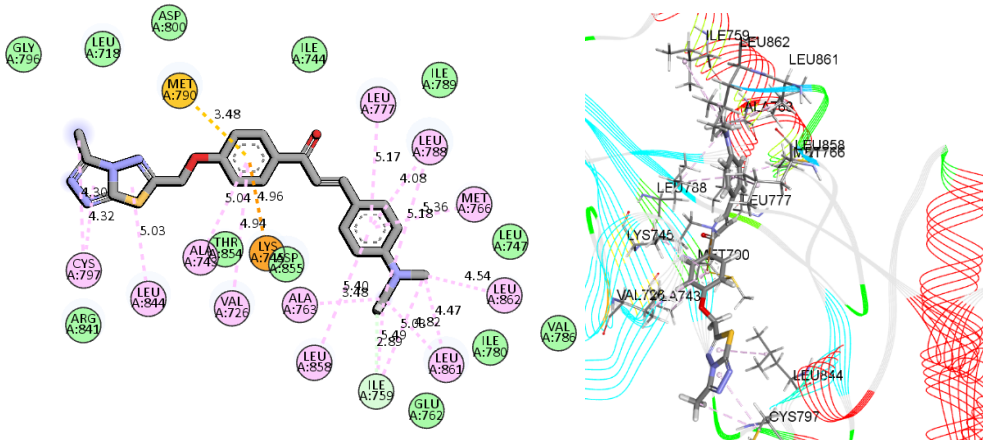

Fig. 5. Visualization of the interactions of the most active molecule (C)

3.3.2. Results of co-crystallized ligand interactions

Analysis of the molecular docking results reveals that the ligand molecule (Ref) has a high affinity for the target protein, with predominant interactions of the hydrogen bonding, electrostatic, and hydrophobic types (Figure 6).

Hydrogen bonding:

A notable hydrogen bond is observed between the H14 atom of the Ref molecule and the oxygen atom (OD2) of aspartic amino acid 800 (ASP800) of the target protein, with 2.079 Å, indicating a strong interaction.

Electrostatic interactions:

A pi-anion electrostatic interaction is present between the oxygen atom (O1E1) of glutamate amino acid 804 (GLU804) of the target protein and the pi orbitals of the Ref molecule, with a distance of 4.21873 Å. This interaction involves an attraction between the opposite charges.

Hydrophobic interactions:

Several hydrophobic interactions of the alkyl and pi-alkyl type are observed between the Ref molecule and the amino acids of the target protein. An alkyl-type hydrophobic interaction is present between the carbon atom (C12) of the Ref molecule and the oxygen atom of the amino acid proline 794 (PRO794) of the target protein, with a 2.796 Å distance. An alkyl-type hydrophobic interaction was also observed between the carbon atom (C36) of the Ref molecule and the oxygen atom of the amino acid leucine 718 (LEU718) of the target protein, with a 2.884 Å distance. Other hydrophobic interactions of the alkyl and pi-alkyl type were observed between the Ref molecule and the VAL243, LEU244, ALA453, SER720, ASN842, PRO794, LEU718, LEU844, CYS797, ALA743, VAL726, MET790, LEU844 and LEU718 amino acids of the target protein, with distances of between 2.73471 Å and 5.98221 Å.

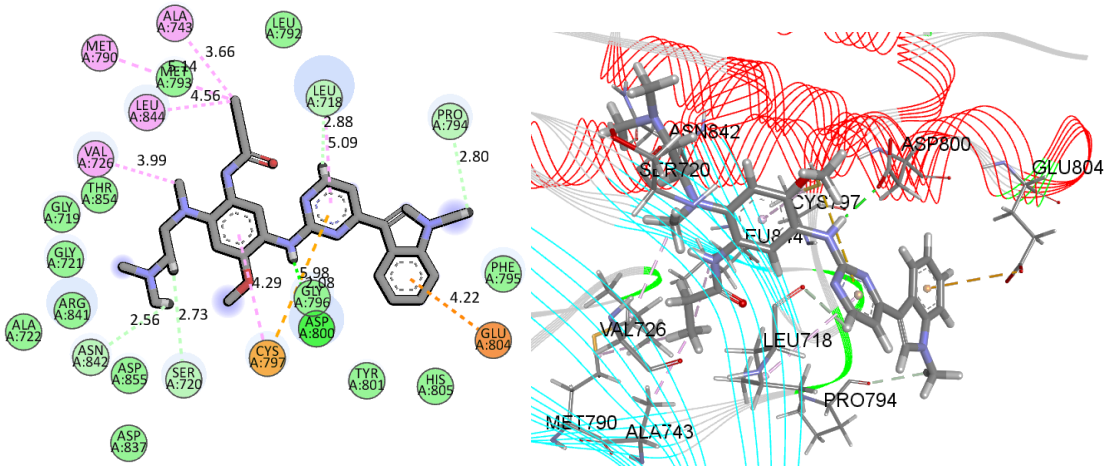

Fig. 6. Visualization of co-crystallized ligand interactions (Ref)

3.3.3. Results of E molecule interactions

The molecular docking results analysis reveals that the ligand molecule (E) has a high affinity for the target protein, with predominant interactions of the hydrogen bonding, electrostatic, and hydrophobic types (Figure 7).

Hydrogen bonding:

A notable hydrogen bond is observed between the H14 atom of E molecule and the oxygen atom (OD2) of the target protein's aspartic amino acid 800 (ASP800), with a 2.079 Å distance, indicating a strong interaction.

Electrostatic interactions:

An electrostatic interaction of the pi-anion type is present between the oxygen atom (O1E1) of the amino acid glutamate 804 (GLU804) of the target protein and the pi orbitals of the E molecule, with a 4.218 Å distance. This interaction involves an attraction between the opposite charges.

Hydrophobic interactions:

Several hydrophobic interactions of the alkyl and pi-alkyl types are observed between molecule E and the amino acids of the target protein.

An alkyl-type hydrophobic interaction is present between molecule E's carbon atom (C12) and the oxygen atom of the amino acid proline 794 (PRO794) of the target protein, with a 2.796 Å distance.

An alkyl-type hydrophobic interaction was also observed between the C36 atom of molecule E and the oxygen atom of the amino acid leucine 718 (LEU718) of the target protein, with a 2.884 Å distance.

Other hydrophobic interactions of the alkyl and pi-alkyl type were observed between molecule E and the amino acids VAL243, LEU244, ALA453, SER720, ASN842, PRO794, LEU718, LEU844, CYS797, ALA743, VAL726, MET790, LEU844 and LEU718 of the target protein, with distances of between 2.73471 Å and 5.98221 Å.

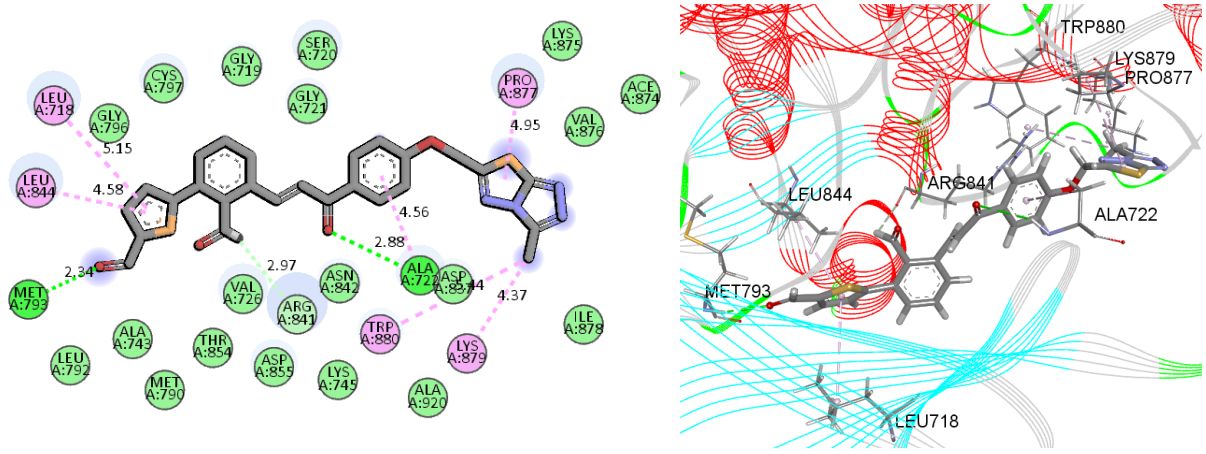

Fig. 7. Visualisation of the interactions of the least active molecule (E)

3.4. ADME-Tox properties

The ADME-Tox properties of the candidate promoters were calculated and evaluated to better understand the pharmacokinetic properties and how the compounds are distributed in the human body, as shown by the results listed in **Table 4**.

Table 4. Predicted ADME-Tox proprieties of the different studied compounds.

Ligands	A	B	D	E	C
Physicochemical Properties					
Molecular weight	394.42 g/mol	489.77 g/mol	514.58 g/mol	504.62 g/mol	421.52 g/mol
Num. heavy atoms	28	29	36	35	30
Num. from. heavy atoms	17	20	25	17	17
Fraction Csp3	0.10	0.10	0.08	0.23	0.23
Num. rotatable bonds	6	6	9	8	7
Num. H-bond acceptors	6	5	7	5	4
Num. H-bond donors	0	0	0	1	1
Molar Refractivity	111.69	117.12	138.50	143.77	122.60
TPSA	96.03 Å²	97.62 Å²	160.00 Å²	136.71 Å²	97.58 Å²
Lipophilicity					
Log $P_{o/w}$ (iLOGP)	-2.71	3.85	3.27	4.12	3.28
Log $P_{o/w}$ (XLOGP3)	4.03	5.25	4.53	6.21	4.58
Log $P_{o/w}$ (WLOGP)	2.26	5.12	5.06	4.39	2.92
Log $P_{o/w}$ (MLOGP)	3.10	3.53	1.83	3.33	2.90
Log $P_{o/w}$ (SILICOS-IT)	1.57	5.71	7.04	5.11	2.71
Consensus Log $P_{o/w}$	1.65	4.69	4.35	4.63	3.28
Water Solubility					
Log *S* (ESOL)	-4.88	-6.30	-5.80	-6.71	-5.30
Solubility	5.23e-03 mg/ml; 1.33e-05 mol/l	2.46e-04 mg/ml; 5.03e-07 mol/l	8.08e-04 mg/ml; 1.57e-06 mol/l	9.79e-05 mg/ml; 1.94e-07 mol/l	2.13e-03 mg/ml; 5.06e-06 mol/l
Class	Moderately soluble	Poorly soluble	Moderately soluble	Poorly soluble	Moderately soluble
Log *S* (Ali)	-5.75	-7.05	-7.61	-8.87	-6.35
Solubility	7.02e-04 mg/ml; 1.78e-06 mol/l	4.37e-05 mg/ml; 8.93e-08 mol/l	1.26e-05 mg/ml; 2.44e-08 mol/l	6.87e-07 mg/ml; 1.36e-09 mol/l	1.87e-04 mg/ml; 4.44e-07 mol/l
Class	Moderately soluble	Poorly soluble	Poorly soluble	Poorly soluble	Poorly soluble
Log *S* (SILICOS-IT)	-5.85	-7.52	-7.70	-6.10	-5.86
Solubility	5.60e-04 mg/ml; 1.42e-06 mol/l	1.49e-05 mg/ml; 3.05e-08 mol/l	1.02e-05 mg/ml; 1.98e-08 mol/l	3.99e-04 mg/ml; 7.91e-07 mol/l	5.82e-04 mg/ml; 1.38e-06 mol/l
Class	Moderately soluble	Poorly soluble	Poorly soluble	Poorly soluble	Moderately soluble
Pharmacokinetics					
GI absorption	High	High	Low	Low	High
BBB permeant	No	No	No	No	No
P-gp substrate	Yes	No	No	No	No
CYP1A2 inhibitor	No	Yes	No	No	No
CYP2C19 inhibitor	Yes	Yes	Yes	Yes	Yes
CYP2C9 inhibitor	No	Yes	Yes	Yes	Yes
CYP2D6 inhibitor	No	No	No	No	Yes
CYP3A4 inhibitor	No	No	Yes	Yes	Yes
Log K_p (skin permeation)	-5.84 cm/s	-5.56 cm/s	-6.22 cm/s	-4.97 cm/s	-5.62 cm/s
Drug likeness					
Lipinski	Yes; 0 violation	Yes; 0 violation	Yes; 1 violation: MW>500	Yes; 1 violation: MW>500	Yes; 0 violation
Ghose	Yes	No; 1 violation: MW>480	No; 2 violations: MW>480, MR>130	No; 2 violations: MW>480, MR>130	Yes
Veber	Yes	Yes	No; 1 violation: TPSA>140	Yes	Yes
Egan	Yes	Yes	No; 1 violation: TPSA>131.6	No; 1 violation: TPSA>131.6	Yes
Muegge	Yes	No; 1 violation: XLOGP3>5	No; 1 violation: TPSA>150	No; 1 violation: XLOGP3>5	Yes
Bioavailability Score	0.55	0.55	0.55	0.55	0.55
Medicinal Chemistry					
PAINS	0 alert	0 alert	0 alert	0 alert	1 alert: anil_di_alk_B
Brenk	2 alerts: michael_acceptor_1, quaternary_nitrogen_1	1 alert: michael_acceptor_1	2 alerts: aldehyde, michael_acceptor_1	2 alerts: aldehyde, michael_acceptor_1	1 alert: michael_acceptor_1
Leadlikeness	No; 2 violations: MW>350, XLOGP3>3.5	No; 2 violations: MW>350, XLOGP3>3.5	No; 3 violations: MW>350, Rotors>7, XLOGP3>3.5	No; 3 violations: MW>350, Rotors>7, XLOGP3>3.5	No; 2 violations: MW>350, XLOGP3>3.5
Synthetic accessibility	4.04	3.59	4.15	5.86	4.36

The calculated physicochemical properties of these molecules show that molecular weight is between 394.42 g/mol (Compound A) and 514.58 g/mol (Compound D), Compound E and Compound C have more saturated regions, while Compound D presents more unsaturation. The most polar molecule is Compound D (TPSA=160.00 Å²), while the most minor polar molecule is Compound A (TPSA 96.03 Å²). Log P O/W is predicted in different ways, and the degree of solubility in water shows that all molecules prefer hydrophobic environments because all molecules are either partially soluble or moderately soluble in water. Compound D, Compound B, and compound E (poorly soluble, high Log P) could be better distributed and absorbed in hydrophobic tissues more than the other two molecules; these characteristics may also facilitate cellular penetration of these three molecules more than the others.

The molecules compound A, compound B, and compound C are strongly absorbed in the intestinal tissue for intestinal absorption. None of these molecules can cross the blood-brain barrier. Compound A can be a P-gp substrate, meaning P-gp can pump it out of cells. All studied molecules inhibit at least one cytochrome involved in drug metabolism, which can cause substantial toxicity to these molecules. Also, these compounds could enter drug interactions with several types of drugs. Compound C represents one PAINS alert. The term "anil_di_alk_B» suggests that there is a structure in the molecule that corresponds to a specific chemical motif; in this case, an aniline with two alkyl groups attached to a specific position in the structure (position B), the PAINS alert is a warning that the presence of this chemical structure in the molecule may cause nonspecific interactions or interference in bioassays. Aniline and alkyl groups can sometimes react nonspecifically with various biological components, leading to biased or unreliable test results. Brenks' alert prediction shows that all the studied structures show at least one alert.

The detected alerts are as follows: "michael_acceptor_1", "quaternary_nitrogen_1," and aldehyde alert; alerts are specific structural motifs used to detect potentially problematic features in a molecule during drug design. The presence of a Michael acceptor can be of concern because it can react nonspecifically with biological nucleophiles; the presence of quaternary nitrogen can also be a warning because these groups can be associated with nonspecific interactions in biological assays. Quaternary nitrogen can sometimes interact with different biological targets, potentially leading to biased test results or undesired interactions in a biological context. Aldehydes can be reactive and participate in various chemical reactions. In the context of drug design, the presence of an aldehyde group can be problematic because these groups can react nonspecifically with biological nucleophiles. Upon comparing the accessibility of synthesizing molecules, A, B, C, D, and E based on the given values (4.04, 3.59, 4.15, 5.86, and 4.36 respectively), it is evident that molecule B, with a value of 3.59, is the easiest to synthesize, indicating less complexity in the preparation process. Molecule A, with a value of 4.04, is slightly more challenging to synthesize than molecule B but is still more accessible than the others. Molecule C, with a value of 4.15, is like molecule A but slightly more challenging to synthesize. Molecule E, with a value of 4.36, is even more challenging to synthesize than molecules A and C, but less complex than molecule D. Finally, molecule D, with a value of 5.86, is the most difficult of the five to synthesize, indicating significant challenges in the preparation process.

3.5. Molecular dynamics simulation results

Fig. 8 shows the RMSD over 100 ns for Protein C-alpha, the complex, and ligand C. The overall upward variations indicate significant conformational changes in the protein structure. The RMSD of the C-alpha protein begins at approximately 1.106 Å and shows a noticeable upward trend, reaching approximately 4.638 Å at 31.2 ns. The ligand's RMSD starts at a relatively low value of 0.278 Å, indicating stable interaction formation initially. However, it peaks at 2.276 Å at 36.4 ns and 1.828 Å at 98 ns, fluctuating from 1.0 to 1.8 Å, suggesting instability or periodic motion in the active site. In contrast, the complex's RMSD starts at 1.69 Å and shows significant fluctuations throughout the simulation, reaching its highest values between 94.4 ns (4.407 Å) and 96.8 ns (4.718 Å). This indicates substantial conformational changes in the complex, possibly due to interactions within the complex or positional changes. The ligand is unstable, with a peak at about 2.4 ns. On the other hand, the RMSD values of the protein and complex show moderate increases at the start of the simulation up to 10 ns, which means they are initially relaxing from their starting shape. During the middle period (10–50 ns), the ligand's RMSD changes significantly, showing short-term motion. At the same time, the RMSD of the protein and complex keeps going up, reaching about 3.6 Å for the protein and 4.2 Å for the complex. The protein's RMSD increases and reaches its maximum values in the late phase (50-100 ns), whereas the complex's RMSD stabilizes at 3–4 Å and reaches a maximum of 4.718 Å. The ligand's relative molecular weight standard deviation (RMSD) exhibits fluctuations but no upward or downward trend.

The protein's RMSD is steadily increasing, indicating significant structural changes possibly due to interactions with the ligand or other nearby molecules. Fluctuations in the complex's RMSD during the experiment have revealed noteworthy structural reorganizations, highlighting the overall dynamic nature of the system. Changes in the ligand's RMSD indicate periods of substantial movement or possible binding events interspersed with stable binding periods.

The protein and complex exhibit remarkable structural dynamics, and the binding of the ligand experiences periods of stability and instability. This analysis demonstrates that the molecular system undergoes substantial conformational changes over time, suggesting dynamic interaction with the active site. In addition to immediate or reoccurring structural analyses, examining these RMSD patterns over time would facilitate the identification of critical conformational states and changes.

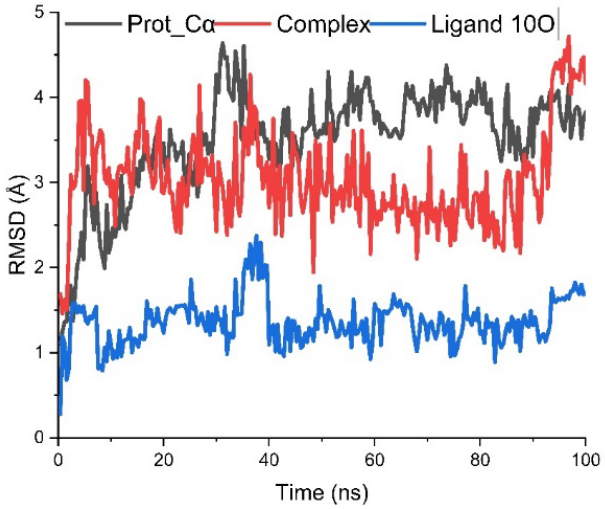

Fig. 8. RMSD of the protein alpha-carbons, complex, and ligand C

The RMSF value of the alpha carbons of the amino acids in the protein is shown on the Y axis of the graph in **Fig. 9**. A high RMSF value indicates that the atom is more mobile, while a low value indicates that it is more rigid. The evolution of the RMSF of each amino acid can be interpreted as follows:

Amino acids with high RMSF (greater than 4Å) are generally located in flexible or disordered regions of the protein. These regions may interact with other solvent molecules, salts, or metals or in more extensive protein movements. Amino acids with a low RMSF (less than 2 Å) are generally located in regions of the protein that form interactions with the C ligand. These regions may be necessary for the stability of the complex.

The protein analysis uncovered interesting information. Amino acids 1 to 50 are rigid and well-structured, with relatively low RMSF. In contrast, amino acids 50 to 100 are more flexible, with higher RMSF. Amino acids 100 to 150 also display low RMSF, indicating another rigid and well-structured region, while amino acids 150 to 200 show higher RMSF, signifying greater flexibility. Moreover, the amino acids 200 to 250 exhibit low RMSF, suggesting another rigid and well-structured region. It is worth noting that the RMSF values of the amino acids interacting with the ligand do not exceed 2 Å, indicating the stability of the ligand within the protein's active site.

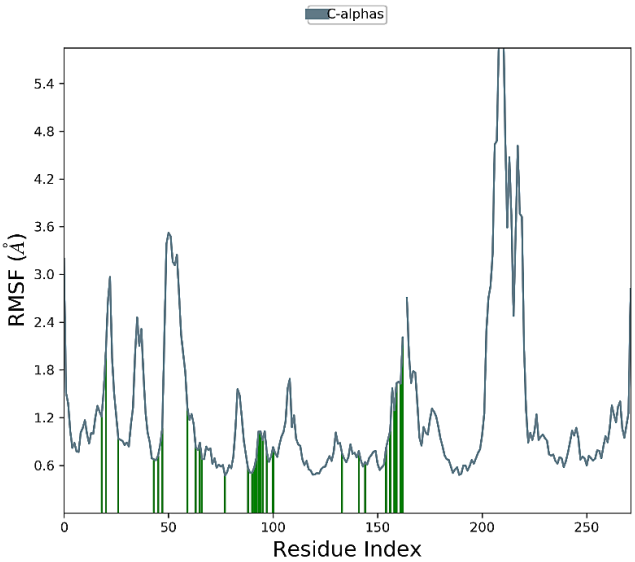

Fig. 9. RMSF of amino acids

The amino acids interact with the ligand C and form different types of bonds: hydrophobic bonds, conventional hydrogen bonds, pi-anion bonds, and water bridges. These bonds are depicted in Figure 10, showing a lack of pi-cationic bonds and a prevalence of hydrophobic bonds. Amino acid LEU718 forms two types of bonds, hydrophobic and water bridges, with a fraction of 0.5, while amino acid CYS 797 forms conventional hydrogen bonds and water bridges, with a fraction of 0.22. Many amino acids predominantly form hydrophobic interactions. Specifically, amino acids MET790, PHE856, SER718, VAL726, LYS745, MET766, and LEU788 exhibit proportions ranging from 0.2 to 0.7.

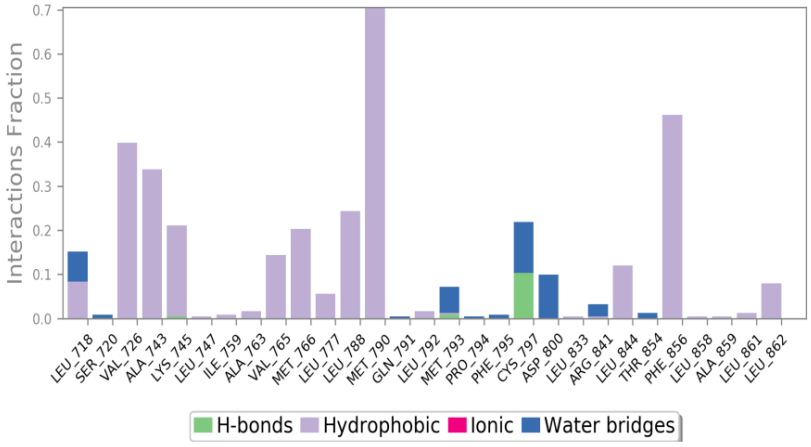

Fig. 10. Ligand C contact with amino acids

Analysis of the RMSF values, as shown in **Fig. 11** for the ligand "C", was conducted with and without the presence of the protein. The results reveal that certain atoms, such as 21, 22, 24, 25, 28, and 30, displayed notably high RMSF values in the presence of the protein, reaching up to 2.987 Å for atom 24 and 2.591 Å for atom 22. It indicates increased flexibility and significant mobility in these regions of the ligand. On the other hand, atoms 6, 8, 9, and 10 exhibited relatively low RMSF values, suggesting increased rigidity and stability in the presence of the protein. Overall, a comparison of the RMSF values with and without the protein generally revealed higher values in the presence of the protein, implying that the protein induces additional flexibility, particularly for atoms 21, 22, 24, and 28. However, certain atoms, such as atom 8, displayed lower RMSF in the presence of the protein, suggesting stabilization of the ligand structure. In summary, the analysis of the RMSF values of the ligand 'C' shows significant differences in the flexibility and stability of the ligand atoms in the presence of the protein, providing essential information for understanding the dynamic interactions between the protein and the ligand. The analysis guides drug design by optimizing the regions of the ligand for optimal interaction with the protein.

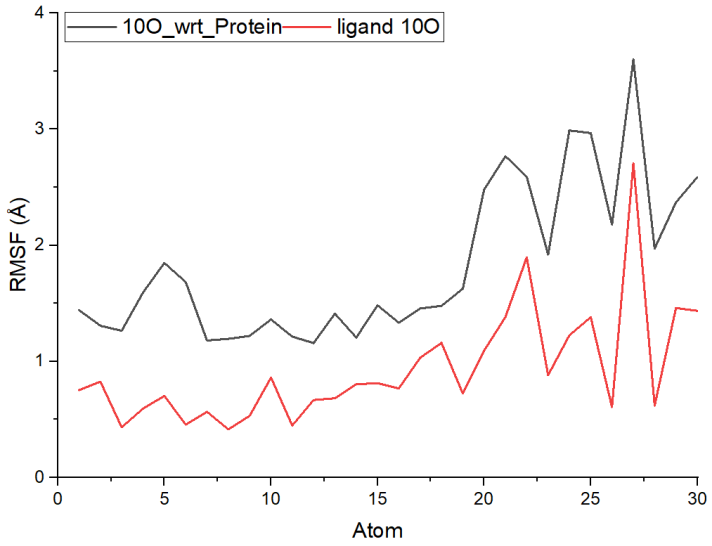

Fig. 11. RMSF of ligand C

The four plots illustrate different aspects of the behaviour of the ligand during a 100 ns dynamic simulation in a critical medium containing solvent (H_2O), salt (NaCl) and normal thermodynamic conditions NVT and NPT. The rGyr is a measure of the overall compactness of a molecule. A high value of rGyr indicates a more extended structure, while a low value indicates a more compact structure. In the case of the ligand C, the rGyr shows some fluctuations during the simulation but remains relatively stable around an average value of about 4 Å. It suggests that the ligand maintains a relatively compact structure during the simulation. SASA is a measure of the solvent-accessible surface area of the molecule. A high value of SASA indicates a more open structure, while a low value indicates a more closed structure. In the case of ligand C, the SASA shows some fluctuation throughout the simulation. However, it remains relatively stable, around an average value of about 300 Å^2. It suggests that the ligand maintains a relatively open structure during the simulation.

The PSA measures the surface area of the molecule made up of polar atoms. A high value of the PSA indicates a more polar structure, while a low value indicates a more non-polar structure. In the case of the C ligand, the PSA shows some fluctuation throughout the simulation. However, it remains relatively stable around an average value of around 100 Å^2. It

suggests that the ligand maintains a relatively polar structure throughout the simulation. MoLSA measures the surface area of the molecule available for hydrophobic interactions. A high MoLSA value indicates a more hydrophobic structure, while a low MoLSA value indicates a more hydrophilic structure. In the case of ligand C, the MoLSA shows some fluctuations during the simulation. However, it remains relatively stable, around an average value of about 200 Å². It suggests that the ligand retains a relatively hydrophobic structure during the simulation. The results of the DM simulation suggest that the C ligand retains a relatively compact, open, polar, and hydrophobic structure during the 100 ns simulation. These properties may influence the ligand's ability to bind to its protein target and exert its biological activity (**Fig. 12**).

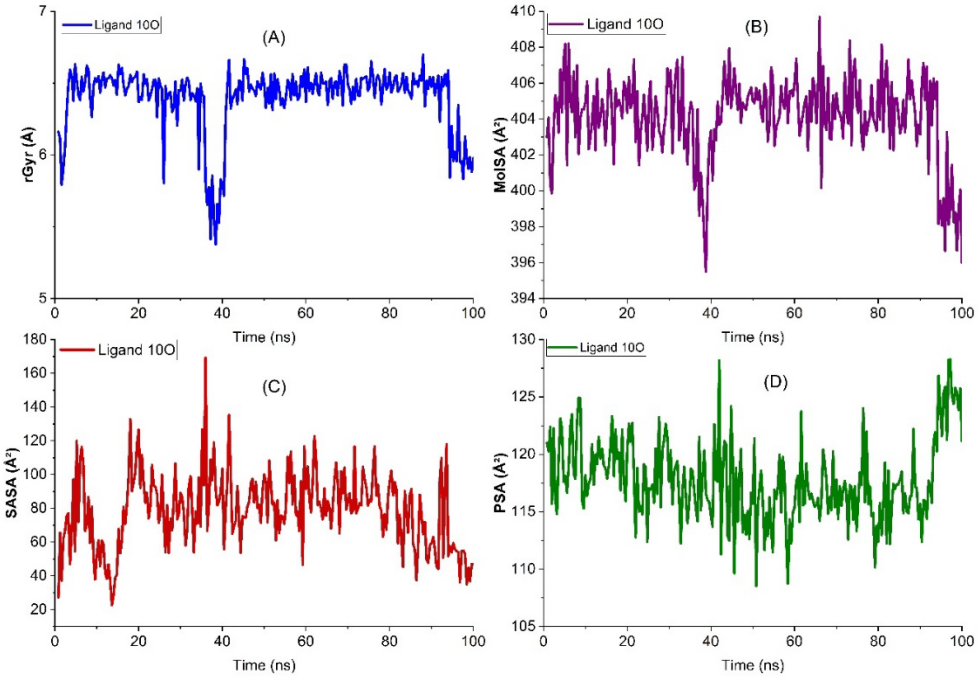

Fig. 12. Properties of ligand C

Table 5. Molecular Mechanics Generalized Born Surface Calculation of Different Types of Energy

Energies	Values (kcal/mol)
ΔG_Bind	-25.14
ΔG_Bind_Coulomb	-0.71
ΔG_Bind_Covalent	-6.30
ΔG_Bind_Hbond	2.63
ΔG_Bind_Lipo	-15.49
ΔG_Bind_Packing	-0.07
ΔG_Bind_vdW	-30.64

The MMGBSA (Molecular et al. Area) results for ligand C show that it contributes to protein binding differently (**Table 5**). The total binding free energy (ΔG_Bind) is -25.14 kcal/mol, indicating a spontaneous and stable ligand-protein interaction. Electrostatic interactions (ΔG_Bind_Coulomb) make a small negative contribution of -0.714 kcal/mol, suggesting a small but beneficial role. Covalent interactions (ΔG_Bind_Covalent) provide a significant stabilizing effect with -6.30 kcal/mol. In contrast, hydrogen bonds (ΔG_Bind_Hbond) positively contribute 2.63 kcal/mol, indicating them to be slightly disadvantageous or energetically expensive. Hydrophobic interactions (ΔG_Bind_Lipo) are significantly favorable with -15.49 kcal/mol, highlighting their crucial role in stabilizing the bond. Packing or steric hindrance (ΔG_Bind_Packing) makes a minimal contribution of -0.07 kcal/mol, indicating minimal influence. Finally, van der Waals interactions (ΔG_Bind_vdW) are the most favorable at -30.644 kcal/mol and play a central role in stabilizing the binding. In conclusion, these results show that the binding of the ligand C to the protein is dominated by hydrophobic and van der Waals interactions, reinforced by covalent interactions. Despite a slightly unfavorable hydrogen bonding, this leads to an overall favorable and stable interaction.

4. Conclusion

Regarding binding affinity, ligands C and E show superior potential to the reference ligands. Detailed studies of ligand C reveal significant interactions with the target protein, including hydrogen bonding and electrostatic and hydrophobic interactions. A critical hydrogen bond is formed between the H46 atom of ligand C and the oxygen of isoleucine 759, contributing to stabilizing the ligand-protein complex. In addition, a significant electrostatic interaction of the pi-cation with lysine 745 and hydrophobic interactions play an essential role in stabilization.

Molecular dynamics simulations show that ligand C retains a compact and stable structure with a total binding free energy (ΔG_Bind) of -25.14 kcal/mol. It indicates a spontaneous and stable interaction. Hydrophobic and van der Waals interactions are the dominant forces in this stabilization, with contributions of -15.49 kcal/mol and -30.64 kcal/mol, respectively.

The analysis of the energy levels shows that the ligand C has a high reactivity, which is attributed to a small energy gap between the HOMO and LUMO levels, allowing for an enhanced biological activity. The presence of dimethylamino groups is significant for inhibiting the antiproliferative activity of cancer cells, known for their electron-donating properties. The high dipole moment of the C molecule (7.018 D) further enhances its biological potential.
Based on its structural and kinetic properties and stabilizing interactions with the EGFR protein, Molecule C appears to be a promising candidate for potential therapeutic uses.

Author Contributions:

Hanane Zaki: Conceptualization, writing – original draft preparation, visualization.
Mohamed Ouabane: Validation, writing – review and editing.
Soumaya Aissaoui: Data analysis, investigation, writing – review and editing.
Marwa Alaqarbeh: Literature review, data collection, writing – review.
Mohammed Bouachrine: Supervision, final validation, project administration.

Funding: This research received no external funding.

Clinical trial registration number: Not applicable.

Acknowledgments

We are grateful to the "*Association Marocaine des Chimistes Théoriciens*" (AMCT) for its pertinent help concerning the programs. This research did not receive any specific funding and was carried out as part of the preparation of the doctoral theses of the students cited in the article.

Statement on conflict of Interest

"The authors declare that they have no competing interests."

References

[1] Elkanzi N. A. A., Hrichi H., Alolayan R. A., Derafa W., Zahou F. M., and Bakr R. B. (**2022**) Synthesis of Chalcones Derivatives and Their Biological Activities: A Review. ACS omega., 7(32) 27769–27786.
[2] Jiang X., Shon K., Li X., Cui G., Wu Y., Wei Z., Wang A., Li X., and Lu Y. (**2024**) Recent advances in identifying protein targets of bioactive natural products. Heliyon., 10 (13) e33917.
[3] WalyEldeen A. A., Sabet S., El-Shorbagy H. M., Abdelhamid I. A., and Ibrahim S. A. (**2023**) Chalcones: Promising therapeutic agents targeting key players and signaling pathways regulating the hallmarks of cancer. Chem. Biol. Interact., 369, 110297.
[4] Ameur S., Barhoumi A., El Alaoui El Abdallaoui H., Syed A., Elalaoui Belghiti M., Elgorban A. M., Wong L. S., Wang S., El Idrissi M., Zeroual A., and Mazoir, N. (**2024**) Molecular docking, exploring diverse selectivities and mechanistic insights in the cycloaddition reaction between 3-benzoylpyrrolo-[1,2-a]quinoxaline-1,2,4(5H)-triones and butyl vinyl ether. Chem Heterocycl Comp., 60, 584–591.
[5] Aitouna A. O., Syed A., Alfagham A. T., Mazoir N., de Julián-Ortiz J. V., Elgorban A. M., El Idrissi M., Wong L. S., and Zeroual A. (**2024**) Investigating the chemical reactivity and molecular docking of 2-diazo-3,3,3-trifluoro-1-nitropropane with phenyl methacrylate using computational methods. Chem Heterocycl Comp., 60 (5) 592–599.
[6] Pitucha M., Janeczko M., Klimek K., Fornal E., Wos M., Pachuta-Stec A., Ginalska G., and Kaczor A. A. (**2020**) 1,2,4-Triazolin-5-thione derivatives with anticancer activity as CK1γ kinase inhibitors. Bioorg. Chem., 99, 103806.
[7] Anil D. A., Aydin B. O., Demir Y., and Türkmenoğlu B. (**2022**) Design, synthesis, biological evaluation and molecular docking studies of novel 1H-1,2,3-Triazole derivatives as potent inhibitors of carbonic anhydrase, acetylcholinesterase and aldose reductase. J. Mol. Struct., 1257.
[8] Hoelm M., Jasiński M. and Palusiak M. A. (**2025**) quantum chemical approach to the physical interpretation of the classical substituent effect in the 2,4-diaryl-4H-1,4-thiazine derivatives. Struct. Chem. **36**, 701–708.
[9] Van Megen M., Reiss G. J., and Frank W. (**2016**) Hydrogen bonding, π-π stacking and van der Waals forces-dominated layered regions in the crystal structure of 4-amino-pyridinium hydrogen (9-phosphono-non-yl)phospho-nate. Acta Cryst. E., 72 (10) 1456–1459.
[10] Ericsson J., Chryssanthou E., Klingspor L., Johansson A. G., Ljungman P., Svensson E., and Sjölin J. (**2013**) Candidaemia in Sweden: A nationwide prospective observational survey. Clin Microbiol Infect., 19 (4) E218-E221.

[11] Ryachi K., Mohammad-Salim H., Al-Sadoon M. K., Zeroual A., de Julián-Ortiz J. V., El Idrissi M., and Tounsi A. (**2024**) Quantum study of the [3+2] cycloaddition of nitrile oxide and carvone oxime: Insights into toxicity, pharmacokinetics, and mechanism. Chem. Heterocycl. Compd., 60 (5) 646–654.

[12] Branco, J., Miranda, I. M., and Rodrigues, A. G. (**2023**) *Candida parapsilosis* Virulence and Antifungal Resistance Mechanisms: A Comprehensive Review of Key Determinants. J. Fungi (Basel)., *9* (1) 80.

[13] Zaki K., Ouabane M., Guendouzi A., Sbai A., Sekkate C., Bouachrine M., and Lakhlifi T. (**2024**) From farm to pharma: Investigation of the therapeutic potential of the dietary plants Apium graveolens L., Coriandrum sativum, and Mentha longifolia, as AhR modulators for Immunotherapy. Comput. Biol. Med., 181, 109051.

[14] Ouabane M., Alaqarbeh M., Hajji H., Tabti K., Ajana M. A., Sbai A., Sekkate C., Lakhlifi T., and Bouachrine M. (**2024**) Quality Control of Coumarins, Furocoumarins and Polymethoxyflavones in Citrus Essential Oils: In Silico Analysis. ChemistrySelect 9 (5) e202303037.

[15] Montagna M. T., Caggiano G., Lovero G., De Giglio O., Coretti C., Cuna T., Iatta R., Giglio M., Dalfino L., Bruno F., and Puntillo F. (**2013**) Epidemiology of invasive fungal infections in the intensive care unit: results of a multicenter Italian survey (AURORA Project). Infection., 41 (3) 645–653.

[16] Becke A. D. (**1988**) Density-functional exchange-energy approximation with correct asymptotic behavior. Physical review. A, General physics., 38 (6) 3098–3100.

[17] Ouabane M., Zaki K., Zaki H., Guendouzi A., Sbai A., Sekkate C., Lakhlifi T., and Bouachrine M. (**2024**) Inhibition of the Janus kinase protein (JAK1) by the *A. Pyrethrum* Root Extract for the treatment of Vitiligo pathology. Design, Molecular Docking, ADME-Tox, MD Simulation, and *in-silico* investigation. Comput Biol Med., 179 (2024) 108816.

[18] Li B. N., Liu Y. Y., Wang Y. P., and Pan M. (**2021**) Visual Detection of Triethylamine and a Dual Input/Output Logic Gate Based on a Eu^{3+}-Complex. Molecules (Basel, Switzerland), 26 (11) 3244.

[19] Belghalia E., Ouabane M., El Bahi S., Rehman H. M., Sbai A., Lakhlifi T., and Bouachrine M. (**2024**) In silico research on new sulfonamide derivatives as BRD4 inhibitors targeting acute myeloid leukemia using various computational techniques including 3D-QSAR, HQSAR, molecular docking, ADME/Tox, and molecular dynamics. Journal of biomolecular structure & dynamics, 42 (17) 9201–9219.

[20] Niggenaber, J., Heyden, L., Grabe, T., Müller, M. P., Lategahn, J., and Rauh, D. (**2020**) Complex Crystal Structures of EGFR with Third-Generation Kinase Inhibitors and Simultaneously Bound Allosteric Ligands. ACS medicinal chemistry letters, 11 (12) 2484–2490.

[21] Meziane H., Abbaoui Z., Ouabane M., Djedouan, A., Chetioui S., El Kodadi M., Touzani R., Hammouti B., Bouachrine M., and Bougueria H. (**2024**) Exploring Phenoxazinone Synthase Activities: Experimental and Theoretical Analyses of Symmetrical Azine Ligands. Phys. Chem. Res.,12 859–868.

[22] Ouabane M., Zaki K., Tabti, K., Alaqarbeh M., Sbai A., Sekkate C., Bouachrine M., and Lakhlifi T. (**2024**) Molecular toxicity of nitrobenzene derivatives to tetrahymena pyriformis based on SMILES descriptors using Monte Carlo, docking, and MD simulations. Comput Biol Med. 169 (2024) 107880.

[23] Ouabane M., Dichane Z., Alaqarbeh M., Alnajjar R., Sekkate C., Lakhlifi T., and Bouachrine M. (**2025**) The use of combined machine learning and in-silico molecular approaches for the study and the prediction of anti-HIV activity. Curr. Chem. Lett., 14 (2025) 205–232.

[24] Althagafi I., El-Metwaly N., and Farghaly T. A. (**2019**) New series of thiazole derivatives: Synthesis, structural elucidation, antimicrobial activity, molecular modeling and MOE docking. Molecules., 24 (9) 1741.

[25] Khaldan A., Bouamrane S., Ouabane M., El-mernissi R., Alaqarbeh M., Alnajjar R., Sönmez Gürer E., Kaya S., Maghat H., Bouachrine M., Lakhlifi T., and Sbai, A. (**2025**) Design, 3D-QSAR, molecular docking, MD simulations, ADME/Tox properties and DFT study of benzimidazole derivatives as promising α-glucosidase inhibitors. J. Mol. Struct., 1328 (2025) 141351.

[26] Qara A., Ouabane M., Sekkate C., Chtita S., Lakhlifi T., and Bouachrine M. (**2024**) Design of New Aromatic Tertiary Amine-based as Butyrylcholinesterase Inhibitors Relying on Molecular Docking, ADME-Tox and Molecular Dynamics. Curr. Comput.-Aided Drug Des., *https://doi.org/10.2174/0115734099302980240722074437*.

[27] Khaldan A., Bouamrane S., El-Mernissi R., Ouabane M., Alaqarbeh M., Maghat H., Ajana M.A., Sekkat C., Bouachrine M., Lakhlifi T., and Sbai A. (**2024**) Design of new α-glucosidase inhibitors through a combination of 3D-QSAR, ADMET screening, molecular docking, molecular dynamics simulations and quantum studies. Arab. J. Chem., 17 (3) 105656.

[28] Ouabane M., Tabti K., Hajji H., Elbouhi M., Khaldan A., Elkamel K., Sbai A., Ajana M. A., Sekkate C., Bouachrine M., and Lakhlifi T. (**2023**) Structure-odor relationship in pyrazines and derivatives: A physicochemical study using 3D-QSPR, HQSPR, Monte Carlo, molecular docking, ADME-Tox and molecular dynamics. Arab. J. Chem., 16 (11) 105207.

[29] En-Nahli F., Hajji H., Ouabane M., Ajana M. A., Sekatte C., Lakhlifi T., and Bouachrine M. (**2023**) ADMET profiling and molecular docking of pyrazole and pyrazolines derivatives as antimicrobial agents. Arab. J. Chem., 16 (11) 105262.

[30] Ouabane, M., Alaqarbeh, M., Hajji, H., Tabti, K., Ajana, M. A., Sbai, A., Sekkate, C., Lakhlifi, T., and Bouachrine, M. (**2024**) Quality Control of Coumarins, Furocoumarins and Polymethoxyflavones in Citrus Essential Oils: In Silico Analysis. ChemistrySelect, 9 (5) e202303037.

[31] Naanaai L., Ouabane M., El Aissouq A., Guendouzi A., Zaitan H., Bouachrine M., and Khalil F. (**2025**) Indole-pyridine carbonitriles as potential anti-diabetic agents: A computational study using 3D-QSAR, molecular docking, ADME-Tox and molecular dynamics simulations. Chem. Afr., 8 (4) 1405–1425.

[32] Elbouhi M., Ouabane M., Tabti K., Badaoui H., Abdessadak O., El Alaouy M. A., Elkamel K., Lakhlifi, T., Sbai A., Ajana M. A., and Bouachrine M. (**2024**) Computational evaluation of 1,2,3-triazole-based VEGFR-2 inhibitors: Anti-angiogenesis potential and pharmacokinetic assessment. J. Biomol. Struct. Dyn., 42 (5) 2549–2559.
[33] Zrinej J., Ouabane M., El Mchichi L., Qara A., Sekkate C., Lakhlifi T., and Bouachrine M. (**2025**) Chemical and biological evaluation of the *Plumbago zeylanica* plant against prostate cancer: A unified approach combining molecular docking, dynamic simulations, pharmacophore modeling, DFT and ADMET studies. Vietnam J. Chem., https://doi.org/10.1002/vjch.70002.
[34] Ouabane M., Zaki K., Zaki H., Guendouzi A., Sbai A., Sekkate C., Lakhlifi T., and Bouachrine M. (**2024**) Inhibition of the Janus kinase protein (JAK1) by the *A. pyrethrum* root extract for the treatment of vitiligo pathology: Design, molecular docking, ADME-Tox, MD simulation, and in-silico investigation. Comput. Biol. Med., 179, 108816.
[35] El Alaouy M. A., Alaqarbeh M., Ouabane M., Sbai A., Lakhlifi T., and Bouachrine M. (**2025**) Computational study of potential MAO-B inhibitors based on 4-(3-nitrophenyl)thiazol-2-ylhydrazone. Turkish Comput. Theor. Chem., 9 (1) 129–156.
[36] Naanaai L., Ouabane M., Moukhliss Y., El Aissouq A., Zaitan H., Bouachrine M., and Khalil F. (**2024**) Design of novel thiazole-based Schiff analogs as α-amylase inhibitors using 3D-QSAR, ADME-Tox, molecular docking, molecular dynamics, biological efficacy, and retrosynthesis. ChemistrySelect, 9 (47) e202404972.
[37] Ouabane M., Zaki K., Alaqarbeh M., Guendouzi A., Sekkate C., Sbai A., Bouachrine M., and Lakhlifi T. (**2024**) Exploring structure–toxicity relationships in nitrobenzene and derivatives: A multifaceted biochemical investigation using 3D–QSPR, HQSPR, molecular docking, and MD simulation. ChemistrySelect, 9 (15) e202304588.
[38] Ouabane M., Zaki K., Tabti K., Alaqarbeh M., Sbai A., Sekkate C., Bouachrine M., and Lakhlifi T. (**2024**) Molecular toxicity of nitrobenzene derivatives to tetrahymena pyriformis based on SMILES descriptors using Monte Carlo, docking, and MD simulations. Comput. Biol. Med., 169 (2024) 107880.
[39] El Alaouy, M. A., El Bahi, S., Boutalaka, M., Ouabane, M., Sbai, A., Maghat, H., Bouachrine, M., and Lakhlifi, T. (**2023**) Organic compounds based on 1-(prop-2-yn-1-ylamino)-2,3-dihydro-1H-indene-4-thiol as selective human monoamine oxidase B inhibitors: Quantitative analysis of structure-activity relationships and in-silico investigations. Mor. J. Chem., 11 (3) 579–896.
[40] Badaoui H., Ouabane M., Alaqarbeh M., Elbouhi M., Choukrad M., Lakhlifi T., and Bouachrine M. (**2025**) The main chemical constituents responsible for the antidiabetic properties of the *Datura metel* L plant: Decryption and in-silico investigations. Phys. Chem. Res., 13 (1) 241-254.
[41] Morris G. M., Goodsell D. S., Halliday R. S., Huey R., Hart W. E., Belew R. K. and Olson A. J. (**1998**) Automated Docking Using a Lamarckian Genetic Algorithm and Empirical Binding Free Energy Function. J. Comput. Chem., 19, 1639-1662.
[42] Nawsheen S., Sufian, M. and Deepa K. (**2019**) Impact of Nicotine Consumption on Hyper Acidic Patients Taking PPI: An *In-Vitro* and Computational Analysis. Health, 11, 129-141.
[43] Trott O., and Olson A. J. (**2010**) AutoDock Vina: improving the speed and accuracy of docking with a new scoring function, efficient optimization, and multithreading. J. Comput. Chem., 31 (2) 455-61.
[44] Lepesheva G. I., Waterman MR. (**2007**) Sterol 14alpha-demethylase cytochrome P450 (CYP51), a P450 in all biological kingdoms. Biochim Biophys Acta. 1770 (3) 467-77.
[45] Slassi S., Zaki H., Amine A., Yamni K., and Bouachrine M. (**2020**) Quantum chemical and molecular docking studies of imidazole and its derivatives as the active antifungal components against *C. albicans*. Phys. Chem. Res., 8 (3) 457–469.
[46] Morrison R. C. (**1992**) The extended Koopmans' theorem and its exactness. J Chem Phys., 96 3718–3722.
[47] Wang H., Wang X., Wang H., Wang L., and Liu A. (**2007**). DFT study of new bipyrazole derivatives and their potential activity as corrosion inhibitors. J. Mol. Model., 13 (1) 147–153.
[48] Baselga J. (**2001**) The EGFR as a target for anticancer therapy—focus on cetuximab. Eur. J. Cancer., 37, 16–22.

© 2025 by the authors; licensee Growing Science, Canada. This is an open access article distributed under the terms and conditions of the Creative Commons Attribution (CC-BY) license (http://creativecommons.org/licenses/by/4.0/).